metals

MDPI

Article

Corrosion Behavior of Pure Ti under a Solid NaCl Deposit in a Wet Oxygen Flow at 600 °C

Lei Fan [1], Li Liu [1,*], Min Cao [1], Zhongfen Yu [2], Ying Li [1,*], Minghui Chen [2] and Fuhui Wang [1,2]

[1] Institute of Metal Research, Chinese Academy of Sciences, Wencui Road 62, Shenyang 110016, China; lfan10s@imr.ac.cn (L.F.); mcao12s@imr.ac.cn (M.C.); fhwang@imr.ac.cn (F.W.)

[2] Key Laboratory for Anisotropy and Texture of Materials (MoE), School of Materials Science and Engineering, Northeastern University, Shenyang 110819, China; zfyu12s@imr.ac.cn (Z.Y.); mhchen@imr.ac.cn (M.C.)

* Correspondence: liliu@imr.ac.cn (L.L.); liying@imr.ac.cn (Y.L.); Tel./Fax: +86-24-2392-5323 (L.L.)

Academic Editor: Hugo F. Lopez

Received: 27 January 2016; Accepted: 17 March 2016; Published: 24 March 2016

Abstract: The corrosion behavior of pure Ti under a solid NaCl deposit in a wet O_2 flow at 600 °C has been studied. The results showed that the corrosion rate was greatly accelerated by solid NaCl, which destroyed the compact and protective TiO_2 scale to yield non-protective $N_4Ti_5O_{12}$ and other products. Detailed scanning electron microscopy (SEM) equipped with an energy dispersive spectrometer (EDX), and X-ray diffraction (XRD) analysis showed that, during the corrosion process, the metal (Ti) diffused outward rapidly and reacted with the wet O_2 to form a thick and porous corrosion products scale. The electrochemical reaction was also observed during the whole corrosion process at 600 °C, which further accelerated the corrosion rate. A possible mechanism has been proposed for pure Ti covered with a solid NaCl deposit in wet O_2 at 600 °C, based on the experimental results.

Keywords: titanium; corrosion; solid NaCl deposit; intermediate temperature; potentiodynamic polarization

1. Introduction

It is widely known that compressor blades suffer more serious corrosion when serving in a marine condition than in an inland condition. This is mainly because, in the marine environment, the working compressor blades are surrounded by moist air, which contains abundant salt (especially NaCl) and water vapor. Since compressor blades generally serve at 300–600 °C (intermediate temperature), NaCl is in solid state and can form a solid deposit layer on the blades surface. As a result, compressor blades would suffer serious corrosion in the simultaneous presence of a solid NaCl deposit layer and wet air.

Under this combined effect of NaCl and wet O_2 at 500–700 °C, the corrosion behavior of several alloys, including Fe-Cr alloys [1], 1Cr11NiW2MoV steel [2], 304 stainless steel [3], and K38G alloy [4], has been extensively studied. To better understand the corrosion mechanism of these alloys, further studies have been conducted to study the corrosion behavior of pure Fe [5–7] and pure Cr [5,8,9], which are the major alloy elements of the blade materials. The results demonstrate that the corrosion rate of pure Fe and pure Cr is sensitive to the presence of a solid NaCl deposit layer because the solid NaCl deposit could react with their oxide at 500–700 °C. This reaction destroys the protective oxide scale formed on the metal surface, and the gathered Cl_2 or HCl reacts with substrate metal cyclically, resulting in a fast corrosion. Additionally, electrochemical reactions have been observed during the corrosion process and were involved in the whole corrosion process [5–7,9]. The interaction of chemical reactions with electrochemical reactions accelerates the corrosion rate significantly.

Titanium alloys are considered appropriate materials for compressor blades because of their superior strength/weight ratio, good creep resistance, and excellent mechanical properties [10,11]. Even some titanium alloys, e.g., Ti-1100 [12], IMI 834 [13], and Ti60 [14], have been used in the compressor at 600 °C (which is the highest serving temperature for compressor blades in application).

The corrosion behavior of titanium alloys under the combined effect of a solid NaCl deposit layer and water vapor at 500–700 °C has been already studied [14–16]. Compared with the good corrosion resistance at room temperature [17–20], titanium alloys, on the other hand, suffer a serious corrosion at 600 °C [14–16]. Additionally, the element Ti, the main alloy element for titanium alloys, is sensitive with solid NaCl at 600 °C, and its oxide (TiO_2) forms the main corrosion products. Thus, in order to reach a clear understanding on the corrosion mechanism of titanium alloys in the serving condition of compressor blades and on the corrosion behavior of element Ti in the whole corrosion process of titanium alloys, it is necessary to study the corrosion behavior of pure Ti under the combined effect of a solid NaCl deposit layer and wet O_2 at 600 °C in details.

In this paper, the corrosion behavior of pure Ti underneath a solid NaCl deposit layer in wet O_2 flow has been investigated at 600 °C using scanning electron microscopy (SEM) equipped with an energy dispersive spectrometer (EDS), X-ray diffraction (XRD), and *in situ* electrochemical measurement. Possible mechanisms have been discussed based on the experimental results.

2. Materials and Methods

The material used in this study was pure Ti, and the samples were cut into pieces of 10 mm × 15 mm × 2 mm. All the samples were mechanically ground to 800 grit (including the edges rounded off) with SiC paper, cleaned in alcohol, and dried in the air. By repeatedly brushing and drying a NaCl-saturated aqueous solution onto the preheated samples [1–4,8,14], a solid NaCl layer was deposited on the sample surface. In this work, the amount of deposited NaCl was about 4 ± 0.2 mg/cm^2.

The corrosion tests were carried out in a thermo-balance [1–4,8,14]. Thermo-gravimetric analysis (TGA) was applied to record the continuous mass gain during the corrosion experiment. The corrosion atmosphere (wet O_2) was obtained by bubbling pure O_2 into distilled water in a glass bubbler (in this study, the flow rate of pure O_2 was about 140 mL/min when the inner diameter of the tube was about 3.2 cm). The volume fraction of water vapor was controlled by adjusting the temperature of distilled water in the glass bubbler. In this study, the temperature of distilled water was about 60 °C, producing a wet O_2 flow with 19.6 vol % water vapor. To prevent the water vapor from condensing inside the thermo-balance, a counter flow of pure N_2 was passed through the thermo-balance. After the furnace reached the desired temperature (600 °C), and the flows of wet O_2 and pure N_2 stabilized, the sample was quickly lowered into the constant temperature zone of the furnace tube.

In this work, the corrosion experiments were conducted under the following corrosion environments: solid NaCl deposit layer in a wet O_2 flow at 600 °C (NWO600); solid NaCl deposit layer in a dry O_2 flow at 600 °C (NO600); wet O_2 flow at 600 °C (WO600); and dry O_2 flow at 600 °C (O600). The specific environmental parameters have been presented in Table 1.

Table 1. Experimental parameters.

Environment	Mass of NaCl (mg/cm^2)	Amount of Water Vapor (vol %)	Flow Rate of O_2 (mL/min)	Temperature (°C)
NWO600	4.0	19.6	140	600
NO600	4.0	0	140	600
WO600	0	19.6	140	600
O600	0	0	140	600

After corrosion, the surface and the cross-sectional morphologies of the samples were collected by SEM/EDX. The chemical composition of corrosion products was investigated by XRD.

A special three-electrode system was built for the *in situ* electrochemical measurements in this particular environment (shown in Figure 1) [6]. To decrease the resistance of the solution and achieve a uniform electric field, the reference electrodes consisted of four platinum wires with a diameter of 0.5 mm, and the counter electrode was a circular strip of platinum foil about 0.2 mm wide. All potential values in this paper were reported *versus* this platinum reference electrode. The working electrode,

pure Ti, was a rod with a length of 10 mm and a diameter of 5 mm. The three electrodes were in quartz tubes, which acted as insulators. All the gaps were sealed by a high temperature inorganic glue [6,7,9]. To decrease the interference of the furnace electric current, the connection wire was covered with a metal shielding layer. After deposited a solid NaCl layer, the three-electrode system was directly put into the furnace at the desired temperature for *in situ* electrochemical measurements.

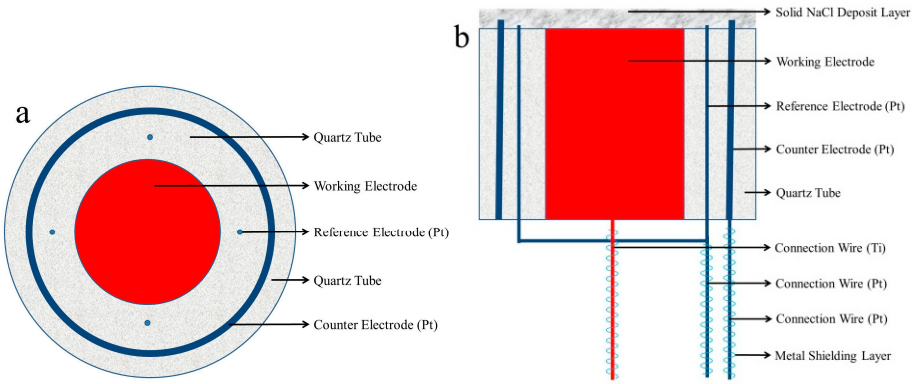

Figure 1. Schematic diagram of three-electrode cell: (**a**) the top view and (**b**) the cross-section view.

The PAR2273 Electrochemical Measurement System manufactured by EG & G was used for all the electrochemical measurements, which also has the ability to compensate the resistance between reference electrode and working electrode. In galvanic corrosion measurement, the ratio of anodic area to cathodic area is 1:2. All the electrochemical measurements were repeated at least three times.

3. Results

3.1. Gravimetry

The mass gain curves of pure Ti under different conditions are shown in Figure 2. The results indicate that, in the absence of the solid NaCl deposit (O600 and WO600), the mass gain of pure Ti is very low during the testing time (20 h). Particularly, the mass gain in WO600 is a little larger than in O600; thus, the water vapor slightly accelerates the corrosion rate of pure Ti without NaCl. In contrast, the mass gain in NO600 and NWO600 increases by a factor of approximate 20, compared with the exposure in O600 and WO600. This demonstrates that pure Ti suffers much more serious corrosion in the presence of solid NaCl at 600 °C. In other words, pure Ti is sensitive to the solid NaCl deposit. Furthermore, the mass gain in NWO600 is a little larger than in NO600, which indicates that water vapor further accelerates the corrosion rate of pure Ti in the presence of a solid NaCl deposit.

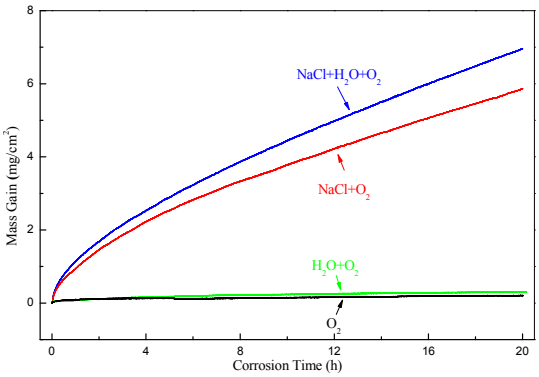

Figure 2. Corrosion kinetics curves of pure Ti under different corrosion environments at 600 °C: (I) dry O_2 (black line), (II) $H_2O + O_2$ (green line), (III) $NaCl + O_2$ (red line), (IV) $NaCl + H_2O + O_2$ (purple line).

3.2. Morphologies and Composition of the Corrosion Products

Figure 3 shows the surface and the cross-sectional morphologies of pure Ti after the samples were exposed in O600 for 20 h. It indicates that a compact and even oxidation scale is formed on the sample surface after 20 h exposure in pure O_2 at 600 °C, and its thickness is about 1 μm. Figure 4 shows the surface and the cross-sectional morphologies of pure Ti after the samples were exposed in WO600 for 20 h. These morphologies (Figure 4a–c) present that the oxidation scale is compact and even. As shown in Figure 4c, its thickness is about 1.5 μm, which is a little thicker than that of O600 (Figure 3c). This means that pure Ti suffers more serious corrosion in the wet O_2 flow, which agrees with the results of the mass gain in Figure 2. Furthermore, when pure Ti is exposed in the wet O_2, the oxidation scale is layered and can be divided into two layers: the inner layer and the outer layer. The inner layer is compact, and its thickness is about 0.5 μm. The outer layer is porous (containing hole marked in Figure 4c), and its thickness is about 1 μm.

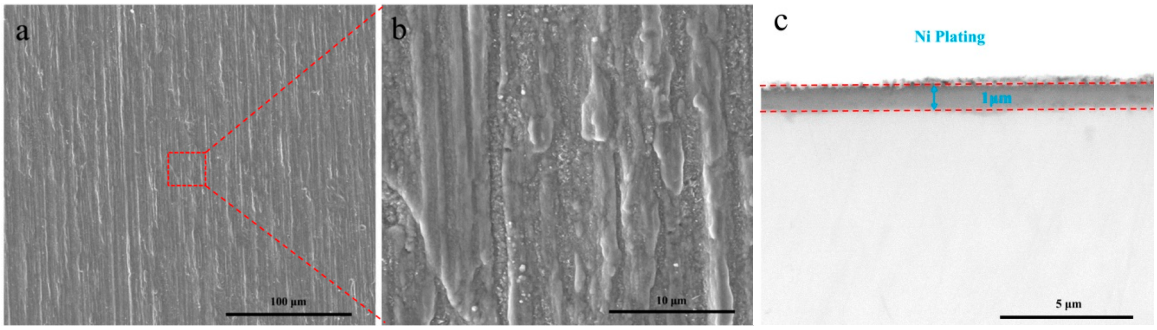

Figure 3. Surface morphologies (**a**); high magnification image (**b**) and cross-sectional morphologies (**c**) of pure Ti oxidized in dry O_2 at 600 °C for 20 h.

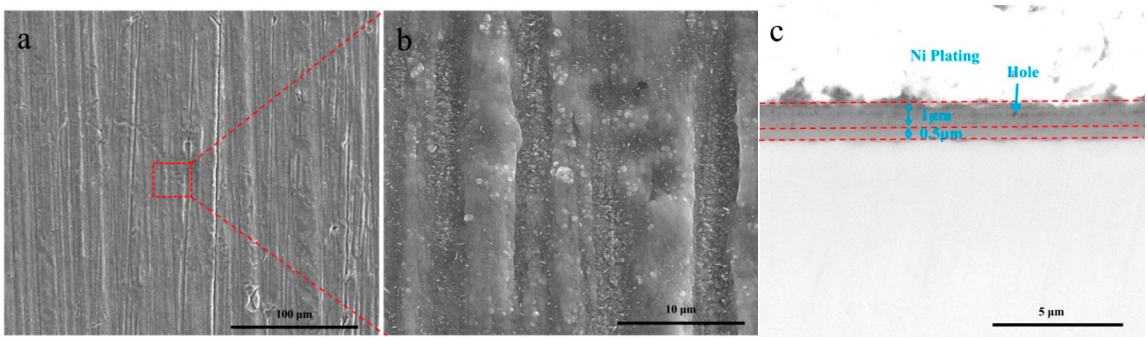

Figure 4. Surface morphologies (**a**); high magnification image (**b**) and cross-sectional morphologies (**c**) of pure Ti oxidized in wet O_2 at 600 °C for 20 h.

The surface and the cross-sectional morphologies of pure Ti after 20 h exposure in NO600 are shown in Figure 5. It can be observed that the corrosion product scale contains the compact structure products and the grid structure products. The compact structure products (marked in Figure 5a,b) are very complete and uniform. The grid structure products (marked in Figure 5a,b) contain lots of through holes (filled with Ni plating, as shown in Figure 5b) penetrating the corrosion scale. These through holes are the fast diffusion path for corrosion medium. Underneath the corrosion scale, a loose layer, containing some holes (close pores), is formed within the substrate due to the diffusion outward of Ti. The thickness of the corrosion products scale is about 60 μm, while that of the loose layer is about 12 μm.

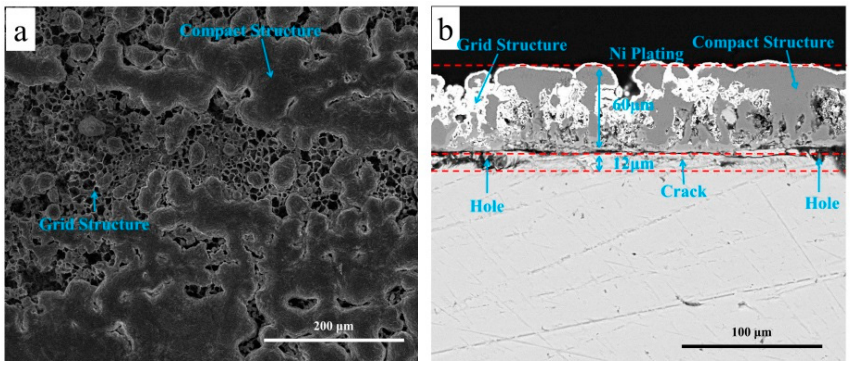

Figure 5. Surface morphologies (**a**) and cross-sectional morphologies (**b**) of pure Ti under a solid NaCl deposit layer in dry O_2 at 600 °C for 20 h.

Figure 6 shows the surface and the cross-sectional morphologies of pure Ti after 20 h exposure in NWO600. The results indicate that the corrosion products scale also contains the compact structure products and the grid structure products. Compared with that one formed in NO600 (Figure 5), the compact structure products are relatively looser and lumpier in NWO600, and the grid structure products contain more through holes. Additionally, a loose layer is formed under the corrosion scale, and its thickness is about 15 μm. Compared with exposure in NO600, this loose layer forming in NWO600 is thicker and contains more and larger holes and cracks. Hence, there are more Ti diffusing outward, and the corrosion is more serious in the simultaneous presence of a solid NaCl deposit and water vapor, which is consistent with the results of mass gain in Figure 2.

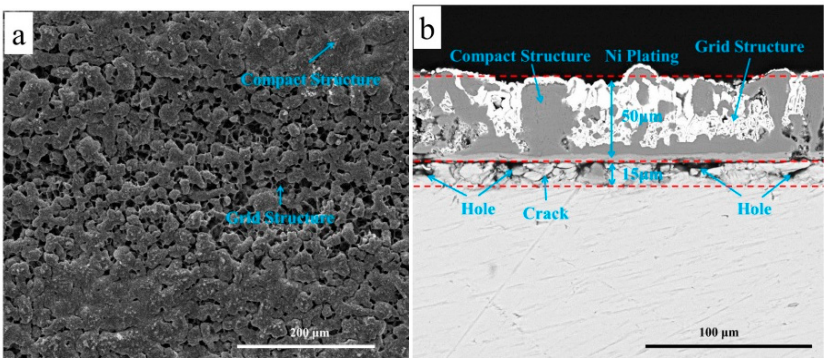

Figure 6. Surface morphologies (**a**) and cross-sectional morphologies (**b**) of pure Ti under a solid NaCl deposit layer in wet O_2 at 600 °C for 20 h.

Figure 7 shows the XRD patterns of the corrosion products. Figure 7a shows that only TiO_2 is formed on the surface of pure Ti after 20 h exposure in O600 and WO600 (pure Ti identified in Figure 7a is the substrate). The XRD patterns in Figure 7b show that, when pure Ti is exposed in the presence of a solid NaCl deposit (NO600 and NWO600), a mixture of corrosion products (containing $Na_4Ti_5O_{12}$ and TiO_2) forms on the sample surface with some residual NaCl. In Figure 7b, it also appears that the intensity of diffraction peaks of $Na_4Ti_5O_{12}$ is larger in NWO600 than in NO600. This means that the water vapor enhances the formation of $Na_4Ti_5O_{12}$ in the presence of a solid NaCl deposit.

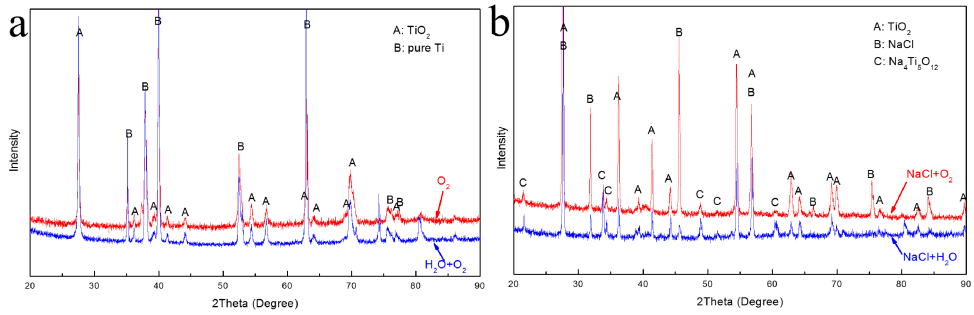

Figure 7. X-ray diffraction patterns of pure Ti oxidized in dry O_2 and wet O_2 up to 20 h at 600 °C (**a**) and X-ray diffraction patterns of pure Ti under a solid NaCl deposit layer in dry O_2 and wet O_2 at 600 °C for 20 h (**b**).

3.3. Electrochemical Corrosion

Figure 8 shows the galvanic corrosion current (I_g) as a function of time for the Pt–Pt couple under NWO600 and the Ti–Pt couple under NWO600. In Figure 8a, I_g of the Pt–Pt couple under NWO600 increases quickly to 7×10^{-7} A/cm^2 in the early stage due to the increase of test temperature and then decreases form the top to -2×10^{-8} A/cm^2 with time varying from 0 to 5 h. I_g of the Ti–Pt couple under NWO600 (Figure 8b) is also divided into a fast increase stage and then a decrease stage. I_g of the Ti–Pt couple under NWO600 is about three orders of magnitude larger than that of the Pt–Pt couple under NWO600, with the maximum value about 1.7×10^{-4} A/cm^2.

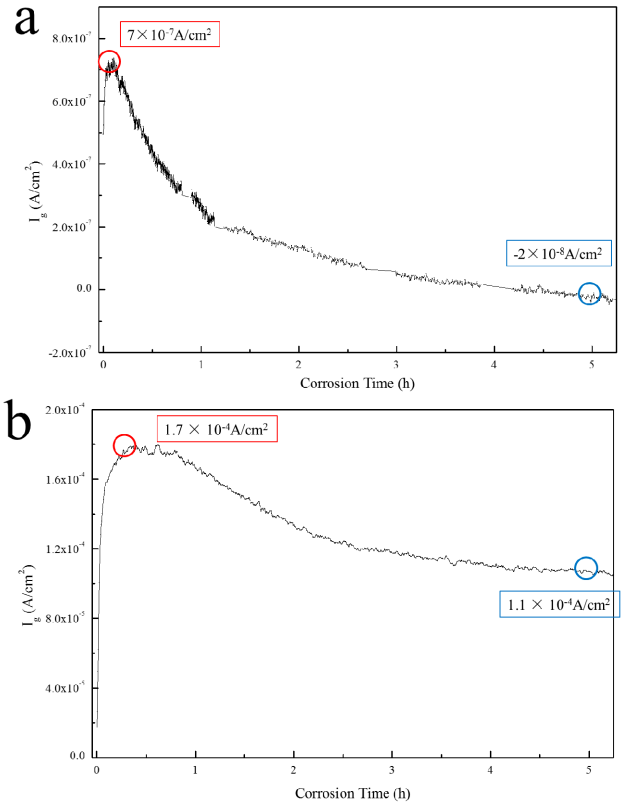

Figure 8. Galvanic corrosion current of the Pt–Pt couple (**a**) and Ti–Pt couple (**b**) under a solid NaCl deposit layer in wet O_2 at 600 °C.

The variation of open circuit potential (E_{OCP}) with corrosion time for pure Ti under NWO600 is presented in Figure 9 and show that E_{OCP} increases quickly to −0.35 V *vs.* Pt in the early stage due to

the increase of test temperature, and then it always declines with corrosion time to −0.6 V *vs.* Pt after 20 h exposure.

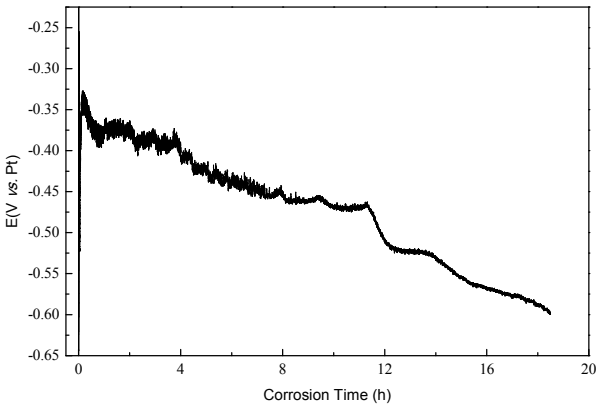

Figure 9. Open circuit potential of the Ti–Pt couple under a solid NaCl deposit layer in wet O_2 at 600 °C.

4. Discussion

4.1. Electrochemical Reaction in the Corrosion Process of Pure Ti under a Solid NaCl Deposit

When pure Cr and pure Fe were exposed in a marine condition at 600 °C, the electrochemical reactions, observed by Liu *et al.* [5] and Tang *et al.* [6,7,9], were involved in the whole corrosion process; thus, the entire corrosion included electrochemical corrosion and chemical corrosion. The electrochemical corrosion was weak but accelerated the corrosion rate greatly by interacting synergistically with the chemical corrosion [6,7,9]. For pure Ti, the measured I_g of the Ti–Pt electrodes under NWO600, which is 1.7×10^{-4} A/cm^2 as shown in Figure 8c, is significantly larger than that of the Pt–Pt electrodes, which is near to zero as shown in Figure 8a. Since no electrochemical reaction occurs on the Pt–Pt electrodes under NWO600 [5,6], its I_g is believed to be the background current density of the whole electrochemical system. Additionally, the value of the measured I_g for the Ti–Pt electrodes is close to the normal electrochemical reaction in the solution. Therefore, it is believed that electrochemical reactions should occur with pure Ti, and electrochemical corrosion is considered to be involved in the corrosion process of pure Ti under NWO600, which is similar with the results of pure Cr [9] and pure Fe [6,7] exposed in the same condition. This means that the entire corrosion of pure Ti under NWO600 includes the electrochemical corrosion reaction and the chemical oxidation reaction.

The percentage of the electrochemical corrosion to the total corrosion (ratio of electrochemical corrosion rate to total corrosion rate) was calculated, because it provides useful insight into the corrosion behavior of pure Ti in the presence of a solid NaCl deposit at 600 °C. The total corrosion rate (consumption of Ti over the entire corrosion) can be calculated by mass gain measurements. The ratio of atom Ti to atom O is assured for the oxidation product, since the oxidation product is approximately TiO_2 (as shown in Figure 7b). Additionally, the corrosion product is mainly composed of oxygen, involved in the corrosion process, and the metal, consumed by corrosion. Thus, the total corrosion rate of the consumed metal (Ti) can be determined from the slope of the mass gain results (Figure 2) according to the ratio of atoms. The electrochemical corrosion rates (consumption of Ti through the electrochemical reaction) can be calculated from the corrosion current density (I_{corr}) which is obtained by fitting the potentiodynamic polarization curves (Figure 10) in the cathodic active polarization zones. The calculation method is described in detail in [9] and the obtained results are presented in Table 2. When pure Ti is exposed in NWO600 respectively for 1 h, the percentage of the electrochemical corrosion to the total corrosion is about 2.43%, while it is about 4.88% after 20 h of exposure.

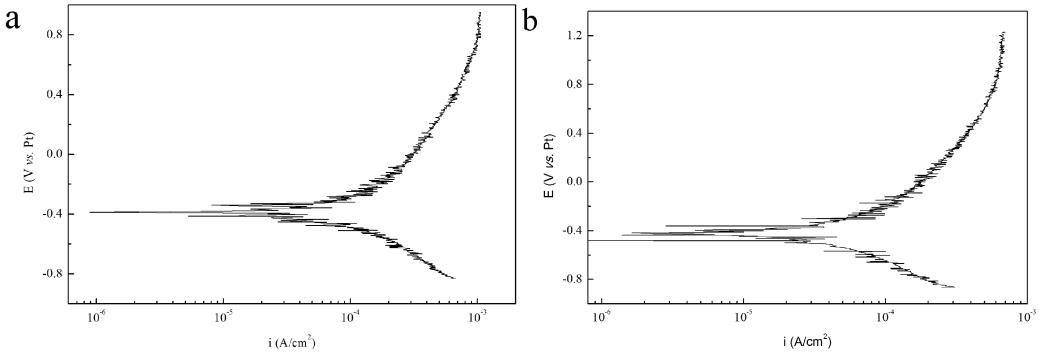

Figure 10. Potentiodynamic polarization plot of the pure Ti under a solid NaCl deposit layer in wet O_2 at 600 °C for 1 h (**a**) and 20 h (**b**).

Table 2. Electrochemical corrosion potential (E_{corr}), electrochemical corrosion rates (I_{corr}), and percentage of electrochemical corrosion to total corrosion of pure Ti under a NaCl deposit in wet O_2 at 600 °C for 1 and 20 h.

Condition	Corrosion Time (h)	E_{corr} (V *vs.* Pt)	I_{corr} (A/cm^2)	Percentage of Electrochemical Corrosion to Total Corrosion
NWO600	1	−0.388	5.04×10^{-5}	2.43%
NWO600	20	−0.436	3.02×10^{-5}	4.88%

We could conclude from this that the electrochemical corrosion occurs during the whole corrosion process in NWO600, but its ratio to total corrosion is very low (less than 5%).

4.2. Corrosion Behavior of Pure Ti under a Solid Deposit

The corrosion is slight when pure Ti is exposed in dry O_2 without NaCl at 600 °C (Figure 2) due to an even, continuous and compact TiO_2 scale formed on the surface (Figure 3). This scale protects the substrate from corrosion.

$$Ti + O_2 = TiO_2 \quad (1)$$

When pure Ti is exposed in the presence of water vapor without NaCl, the oxidation rate is amplified slightly (Figure 2), and a layered and thicker oxide scale is formed on the sample surface (Figure 4c). Additionally, the results of XRD (Figure 7a) indicate that the corrosion product is only TiO_2. Thus, we can conclude that the composition and the crystal structure of the oxide scale are even, and the difference between the two layers is just their compactness. At high temperature, H_2O tends to dissociate at the defects on TiO_2/(110) planes into free H atoms and OH groups [21–23]. The generated hydrogen atoms are more prone to diffuse into TiO_2 through the crystal channels in the c-axis direction, along which the diffusion rate is at least one order of magnitude larger than that in the direction perpendicular to c-axis [21,22]. This dissolution of hydrogen in TiO_2 can increase the concentration of crystal defects by forming hydrogen defects, thereby increasing the diffusion outward of Ti ions [23]. This fast diffusion in the scale result in a larger corrosion rate and the hole formed in the oxide scale (marked in Figure 4c), which leads to a thicker and more porous layer (Figure 4c).

When pure Ti is covered with a solid NaCl deposit layer, the corrosion rate is seriously accelerated (Figure 2) since the corrosion product scale is non-protective and the protective TiO_2 scale cannot be formed in the presence of a solid NaCl deposit (Figure 5a,b). The protective TiO_2 scale cannot form due to the occurrence of a series of chemical reactions, which are the main actors during the whole corrosion, and lead to an active corrosion. Firstly, the TiO_2 scale reacts with NaCl and O_2 [14], which destroys the protective scale:

$$5TiO_2 + 4NaCl + O_2 = Na_4Ti_5O_{12} + 2Cl_2 \quad (2)$$

Additionally, this destructive reaction can occur as following:

$$6TiO_2 + 4NaCl = Na_4Ti_5O_{12} + TiCl_4 \quad (3)$$

$$TiCl_4 + O_2 = TiO_2 + 2Cl_2 \quad (4)$$

The generated Cl_2 in Reactions (2) or (4) diffuses inward quickly through the through holes in the porous corrosion products scale (Figure 5b) and reacts with the substrate (Ti) [2,8,14].

$$Cl_2 + Ti = TiCl_2 \quad (5)$$

$$2Cl_2 + Ti = TiCl_4 \quad (6)$$

Due to high vapor pressure and high activity at 600 °C, $TiCl_2$ and $TiCl_4$ diffuse outward quickly and react with O_2 immediately [14] through the following reaction and Reaction (4) respectively.

$$TiCl_2 + O_2 = TiO_2 + Cl_2 \quad (7)$$

The standard Gibbs free energy changes (ΔG°) of these reactions at 600 °C are presented in Table 3. ΔG° of these reactions are negative; thus, the reactions are thermodynamically spontaneous. The generated Cl_2 in Reactions (4) and (7) can diffuse inward and react with substrate again. Thus, Cl_2 reacts with the substrate cyclically, resulting in the diffusion outward of the metal (Ti) forming the hole and the cracks in the loose layer as shown in Figure 5b and the fast corrosion. Additionally, TiO_2 is mainly formed by the chemical sedimentation of the Reactions (4) and (7), and the gaseous species (Cl_2, $TiCl_2$, and $TiCl_4$) are produced in the corrosion process; therefore, the produced TiO_2 is porous and non-protective.

Table 3. Standard Gibbs free energy changes of reactions at 600 °C.

Reaction	ΔG° kJ/mol
$Ti + O_2 \rightarrow TiO_2$	−785
$4NaCl + 5TiO_2 + O_2 \rightarrow Na_4Ti_5O_{12} + 2Cl_2$	−194
$4NaCl + 6TiO_2 \rightarrow Na_4Ti_5O_{12} + TiCl_4$	−65
$TiCl_4 + O_2 \rightarrow TiO_2 + 2Cl_2$	−129
$Ti + Cl_2 \rightarrow TiCl_2$	−374
$Ti + 2Cl_2 \rightarrow TiCl_4$	−656
$TiCl_2 + O_2 \rightarrow TiO_2 + Cl_2$	−411
$4NaCl + 5TiO_2 + 2H_2O \rightarrow Na_4Ti_5O_{12} + 4HCl$	−195
$TiCl_4 + 2H_2O \rightarrow TiO_2 + 4HCl$	−130
$Ti + 2HCl \rightarrow TiCl_2 + H_2$	−174
$Ti + 4HCl \rightarrow TiCl_4 + 2H_2$	−256
$2TiCl_2 + 2H_2O + O_2 \rightarrow 2TiO_2 + 4HCl$	−905
$2H_2 + O_2 \rightarrow 2H_2O$	−399

In the presence of water vapor, the corrosion rate of pure Ti under a solid NaCl deposit is a little larger than that without H_2O (Figure 2). The corrosion mechanism is similar to that in NO600 and discussed as following.

$$5TiO_2 + 4NaCl + 2H_2O = Na_4Ti_5O_{12} + 4HCl \quad (8)$$

$$TiCl_4 + 2H_2O = TiO_2 + 4HCl \quad (9)$$

$$2HCl + Ti = TiCl_2 + H_2 \quad (10)$$

$$4HCl + Ti = TiCl_4 + 2H_2 \quad (11)$$

$$2TiCl_2 + O_2 + 2H_2O = 2TiO_2 + 4HCl \quad (12)$$

$$2H_2 + O_2 = 2H_2O \quad (13)$$

$TiCl_4$ in the Reaction (9) is produced through Reaction (3). These reactions are also thermodynamically spontaneous due to the negative ΔG°, as presented in Table 3. Thus, NaCl destroys the protective scale through Reactions (3) and (8), and HCl reacts with the substrate cyclically. Due to the higher activity of HCl than that of Cl_2, the rates of Reactions (10) and (11) are larger than Reactions (5) and (6). Additionally, the concentration of crystal defects is greater by forming hydrogen defects due to the dissolution of H_2O into TiO_2 as previously discussed. Thus, more Ti is consumed and then diffused outward, resulting in larger corrosion rate (Figure 2) and looser corrosion products scale (Figure 6). This higher consumption of Ti also results in a thicker loose layer with more holes and cracks underneath the corrosion product scale as shown in Figure 6b.

$TiCl_4$, $TiCl_2$, Cl_2, HCl, and H_2 act repeatedly in the reaction and have a very short lifetime. Thus, it is difficult to exactly identify the chemical species.

On the other hand, the electrochemical corrosion occurs during the whole corrosion process when pure Ti is exposed in NWO600, which has been discussed. For pure Ti, the anodic reaction is simple.

$$Ti = Ti^{4+} + 4e \quad (14)$$

This anodic reaction could enhance the consumption of metal (Ti) in the corrosion process; thus, the electrochemical reaction maybe further aggravate the corrosion in NWO600.

5. Conclusions

The corrosion rate of pure Ti under a solid NaCl deposit in a wet O_2 flow at 600 °C was greatly amplified by the solid NaCl. The corrosion product scale is very porous and thick in the presence of solid NaCl. We believe that solid NaCl reacts with Ti oxides to form $Na_4Ti_5O_{12}$, which decreases the protective ability of the corrosion product scale, thereby aggravating the corrosion process. Meanwhile, the electrochemical reaction, which is slight during the whole corrosion process, promotes metal transfer into metal cations and aggravates the corrosion further.

Acknowledgments: This investigation was supported by the National Key Basic Research and Development Plan of China under the Contract No. 2014CB643303, the National Natural Science Foundation of China under the Contract No. 51371181, the National Natural Science Foundation of China under the Contract No. 51531007 and the International S&T Cooperation Program of China (ISTCP) (No. 2014DFR50560).

Author Contributions: The tests were carried out by Lei Fan, characterization was performed by Lei Fan and Li Liu, the experimental scheme was framed by Fuhui Wang. The manuscript was composed by Lei Fan and revised by Li Liu, Min Cao, Zhongfen Yu and Minghui Chen.

Conflicts of Interest: The authors declare no conflict of interest.

References

1. Wang, F.; Shu, Y. Influence of Cr content on the corrosion of Fe-Cr alloys: The synergistic effect of NaCl and water vapor. *Oxid. Met.* **2003**, *59*, 201–214. [CrossRef]
2. Shu, Y.H.; Wang, F.; Wu, W.T. Synergistic effect of NaCl and water vapor on the corrosion of 1Cr-11Ni-2W-2Mo-V steel at 500–700 °C. *Oxid. Met.* **1999**, *51*, 97–110. [CrossRef]
3. Wang, C.; Jiang, F.; Wang, F. Corrosion inhibition of 304 stainless steel by nano-sized Ti/silicone coatings in an environment containing NaCl and water vapor at 400–600 °C. *Oxid. Met.* **2004**, *62*, 1–13. [CrossRef]
4. Wang, F.H.; Geng, S.J.; Zhu, S.L. Corrosion behavior of a sputtered K38G nanocrystalline coating with a solid NaCl deposit in wet oxygen at 600 to 700 °C. *Oxid. Met.* **2002**, *58*, 185–195. [CrossRef]
5. Liu, L.; Li, Y.; Zeng, C.L.; Wang, F.H. Electrochemical impedance spectroscopy (EIS) studies of the corrosion of pure Fe and Cr at 600 °C under solid NaCl deposit in water vapor. *Electrochim. Acta* **2006**, *51*, 4736–4743. [CrossRef]

6. Tang, Y.; Liu, L.; Li, Y.; Wang, F. Evidence for the occurrence of electrochemical reactions and their interaction with chemical reactions during the corrosion of pure Fe with solid NaCl deposit in water vapor at 600 °C. *Electrochem. Commun.* **2010**, *12*, 191–193. [CrossRef]
7. Tang, Y.; Liu, L.; Fan, L.; Li, Y.; Wang, F. The corrosion behavior of pure iron under solid Na_2SO_4 deposit in wet oxygen flow at 500 °C. *Materials* **2014**, *7*, 6144–6157. [CrossRef]
8. Shu, Y.H.; Wang, F.H.; Wu, W.T. Corrosion behavior of pure Cr with a solid NaCl deposit in O_2 plus water vapor. *Oxid. Met.* **2000**, *54*, 457–471. [CrossRef]
9. Tang, Y.B.; Liu, L.; Li, Y.; Wang, F.H. The electrochemical corrosion mechanisms of pure Cr with NaCl deposit in water vapor at 600 °C. *J. Electrochem. Soc.* **2011**, *158*, C237–C241. [CrossRef]
10. Guleryuz, H.; Cimenoglu, H. Oxidation of Ti-6Al-4V alloy. *J. Alloys Compd.* **2009**, *472*, 241–246. [CrossRef]
11. Lee, D.H.; Nam, S.W. High temperature fatigue behavior in tensile hold LCF of near-alpha Ti-1100 with lamellar structure. *J. Mater. Sci.* **1999**, *34*, 2843–2849. [CrossRef]
12. Bredow, T.; Jug, K. Theoretical investigation of water-adsorption at rutile and anatase surfaces. *Surf. Sci.* **1995**, *327*, 398–408. [CrossRef]
13. Wanjara, P.; Jahazi, M.; Monajati, H.; Yue, S.; Immarigeon, J.P. Hot working behavior of near-alpha alloy IMI834. *Mater. Sci. Eng. A* **2005**, *396*, 50–60. [CrossRef]
14. Shu, Y.H.; Wang, F.H.; Wu, W.T. Corrosion behavior of Ti60 alloy coated with a solid NaCl deposit in O_2 plus water vapor at 500–700 °C. *Oxid. Met.* **1999**, *52*, 463–473. [CrossRef]
15. Dumas, P.; Stjohn, C. NaCl-induced accelerated oxidation of a titanium alloy. *Oxid. Met.* **1976**, *10*, 127–134. [CrossRef]
16. Yao, Z.; Marek, M. NaCl-induced hot corrosion of a titanium aluminide alloy. *Mater. Sci. Eng. A* **1995**, *192*, 994–1000. [CrossRef]
17. Delgado-Alvarado, C.; Sundaram, P.A. A study of the corrosion behavior of gamma titanium aluminide in 3.5 wt% NaCl solution and seawater. *Corros. Sci.* **2007**, *49*, 3732–3741. [CrossRef]
18. Kim, H.S.; Kim, W.J. Annealing effects on the corrosion resistance of ultrafine-grained pure titanium. *Corros. Sci.* **2014**, *89*, 331–337. [CrossRef]
19. Kim, J.; Park, H.W. Influence of a large pulsed electron beam (LPEB) on the corrosion resistance of Ti-6Al-7Nb alloys. *Corros. Sci.* **2015**, *90*, 153–160. [CrossRef]
20. Zhi, Q.; Xiaolu, P.; Yu, Y.; Lijie, Q.; Tran, H.T.; Volinsky, A.A. Passive film-induced stress and mechanical properties of alpha-Ti in methanol solution. *Corros. Sci.* **2014**, *78*, 287–292.
21. Johnson, O.W.; Paek, S.H.; Deford, J.W. Diffusion of H and D in TiO_2: Supperssion of internal fields by isotope exchange. *J. Appl. Phys.* **1975**, *46*, 1026–1033. [CrossRef]
22. Fowler, J.D.; Chandra, D.; Elleman, T.S.; Payne, A.W.; Verghese, K.T. Diffusion in Al_2O_3 and BEO. *J. Am. Ceram. Soc.* **1977**, *60*, 155–161. [CrossRef]
23. Douglass, D.L.; Kofstad, P.; Rahmel, A.; Wood, G.C. International workshop on high-temperature corrosion. *Oxid. Met.* **1996**, *45*, 529–620. [CrossRef]